Experimental and theoretical evidence of universality in superfluid vortex reconnections

P. Z. Stasiak,[1] Y. Xing,[2,3] Y. Alihosseini,[2,3] C.F. Barenghi,[1]
A. Baggaley,[1] W. Guo,[2,3] L. Galantucci,[4] and G. Krstulovic[5]

[1]*School of Mathematics, Statistics and Physics, Newcastle University,
Newcastle upon Tyne, NE1 7RU, United Kingdom*
[2]*National High Magnetic Field Laboratory, 1800 East Paul Dirac Drive, Tallahassee, Florida 32310, USA*
[3]*Mechanical Engineering Department, FAMU-FSU College of Engineering, Tallahassee, Florida 32310, USA*
[4]*Istituto per le Applicazioni del Calcolo "M. Picone" IAC CNR, Via dei Taurini 19, 00185 Roma, Italy*
[5]*Université Côte d'Azur, Observatoire de la Côte d'Azur, CNRS,Laboratoire Lagrangre,
Boulevard de l'Observatoire CS 34229 - F 06304 NICE Cedex 4, France*

The minimum separation between reconnecting vortices in fluids and superfluids obeys a universal scaling law with respect to time. The pre-reconnection and the post-reconnection prefactors of this scaling law are different, a property related to irreversibility and to energy transfer and dissipation mechanisms. In the present work, we determine the temperature dependence of these prefactors in superfluid helium from experiments and a numeric model which fully accounts for the coupled dynamics of the superfluid vortex lines and the thermal normal fluid component. At all temperatures, we observe a pre- and post-reconnection asymmetry similar to that observed in other superfluids and in classical viscous fluids, indicating that vortex reconnections display a universal behaviour independent of the small-scale regularising dynamics. We also numerically show that each vortex reconnection event represents a sudden injection of energy in the normal fluid. Finally we argue that in a turbulent flow, these punctuated energy injections can sustain the normal fluid in a perturbed state, provided that the density of superfluid vortices is large enough.

Introduction.— Reconnections are the fundamental events that change the topology of the field lines in fluids and plasmas during their time evolution. Reconnections thus determine important physical properties, such as mixing and inter-scale energy transfer in fluids [1], or solar flares and tokamak instabilities in plasmas [2]. The nature of reconnections is more clearly studied if the field lines are concentrated in well-separated filamentary structures: vortices in fluids and magnetic flux tubes in plasmas. In superfluid helium this concentration is extreme, providing an ideal context: superfluid vorticity is confined to vortex lines of atomic thickness (approximately $a_0 \approx 10^{-10}$ m); a further simplification is that, unlike what happens in ordinary fluids, the circulation of a superfluid vortex is constrained to the quantized value $\kappa = h/m = 9.97 \times 10^{-8}$ m^2/s, where m is the mass of one helium atom and h is Planck's constant.

It was in this superfluid context that it was theoretically and experimentally recognized [3–8] that reconnections share a universal property irrespective of the initial condition: the minimum distance between reconnecting vortices, $\delta^{\pm}$, scales with time, t, according to the form

$$\delta^{\pm}(t) = A^{\pm}(\kappa|t - t_0|)^{1/2}, \tag{1}$$

where t_0 is the reconnection time, and the dimensionless prefactors A^- and A^+ refer respectively to before ($t < t_0$) and after ($t > t_0$) the reconnection. The same scaling law was then found for reconnections in ordinary viscous fluids [9]. In the case of a pure superfluid at temperature $T = 0$ K, theoretical work based on the Gross-Pitaevskii equation (GPE) has shown that $A^+ > A^-$, that is, after the reconnection, vortex lines move away from each others faster than in the initial approach; this result has been related to irreversibility [10, 11]. Indeed, a geometrical constraint imposes [11] that a piece of vortex length needs to be "deleted" during the reconnection process. In the GP model, this loss is possible by the emission of a rarefaction pulse created immediately after the reconnection [6, 12] which removes some of the kinetic energy and momentum of the vortex configuration. This vortex energy loss depends on the ratio A^+/A^-, which in turns defines the approaching angle of collision between the vortices, together with other several geometrical quantities [7, 11].

The temporal asymmetry $A^+ > A^-$ can be thus interpreted as a non-trivial manifestation of irreversibility, as it originates from an ideal hydrodynamic process independent of the small-scale regularisation mechanism of the fluid. Indeed, in classical fluid vortex reconnections, although the definition of A^+ is more delicate as circulation is not necessarily conserved, the same asymmetry $A^+ > A^-$ was reported [9]. Instead of the generation of rarefaction pulses, like in the case of $T = 0$ superfluids, close to the reconnection, the classical fluid creates a series of thin secondary structures that can be then efficiently dissipated by viscous dissipation.

The case of superfluid helium at non-zero temperatures is more intriguing. Most experiments are performed at $T > 1$ K, a regime in which in addition to quantum vortices, thermal excitations constitute a viscous liquid called the *normal fluid*. The normal fluid can steal energy from filaments and dissipate it by viscous effects, opening in that way more routes towards irreversibility. Modern visualisation techniques rely on hydrogen/deuterium tracer particles to
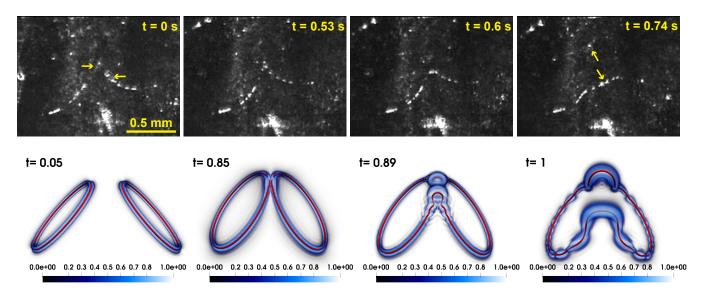
FIG. 1: *Top row:* Images showing tracer particles trapped on reconnecting vortices in superfluid helium at 1.65 K. The arrows denote the vortices before and after the reconnection. The first two images show that the vortices approach each other before the reconnection, which occurs at $t = 0.58$ s. After the reconnection, the resulting vortices start to move apart, as shown in the last two images. *Bottom row:* Oblique collision of two circular vortex rings at different (dimensionless) times, here in units of $\tau = 0.183$s. The superfluid vortex lines are represented by red tubes (the radius has been greatly exaggerated for visual purposes); the scaled normal fluid enstrophy $\boldsymbol{\omega}^2/\boldsymbol{\omega}_{max}^2$ is represented by the blue volume rendering.

.

decorate superfluid vortices [4, 13–15]. Numerous studies have provided insight into the post-reconnection dynamics and the prefactor A^+, but much less is known about A^- from experiments due to the challenges of visualising vortices approaching a reconnection.

The aim of this Letter is to investigate the role played by the normal fluid in the reconnection dynamics. In particular, given the temperature dependence of the normal fluid's properties, we study experimentally and numerically the temperature dependence of the prefactors A^+ and A^- and numerically investigate the energy injected in the normal fluid. To achieve this aim we need a more powerful model than the GPE to account not only for the dynamics of the superfluid vortices, but also for the dynamics of the normal fluid. We show that at non-zero temperatures Eq. (1) and the relation $A^+ > A^-$ hold true, in agreement with experiments, revealing, for the first time, a temperature dependence of A^+/A^-. In addition, we show that a vortex reconnection represents an unusual kind of punctuated energy injection into the normal fluid which acts alongside the well-known (continual) friction. When applied to superfluid turbulence, this last result implies that, if the vortex line density (hence the frequency of reconnections) is large enough, vortex reconnections can maintain the normal fluid in a perturbed state.

Experimental Method.— To visualize the reconnection dynamics, we decorate the vortices using solidified deuterium (D_2) tracer particles of density 202.8 kg/m³ [16]) and mean radius 1.1×10^{-6} m [17, 18]. These particles are generated by injecting a $D_2/^4$He gas mixture into the superfluid helium bath [17, 19] as described in the Supplementary Material (SM). When the particles are near the vortices, they become trapped inside their cores because of the Bernoulli pressure arising from the circulating superfluid flow. A thin laser sheet is used to illuminate the particles, and their motion is recorded at 200 Hz by a camera positioned at a right angle to the laser sheet. A high-quality reconnection event, observed at $T = 1.65$ K and capturing both the pre- and post-reconnection dynamics, is shown in Fig. 1 as an example. Note that according to GP simulations [20] the transfer of energy and momentum between particle and vortex does not modify the approaching rates significantly. Reconnection events reported in this work have been captured in multiple experiments, either following particle injection or long time (*i.e.*, 30-60 s) after towing a grid through superfluid helium. (this is also supported by the scaling symmetry of the system which allows to draw conclusion for length-scales relevant to experiments).

Numerical Method.— We follow the approach of Schwarz [21] which exploits the vast separation of length scales between the vortex core a_0 and any other relevant distance, in particular the average distance between vortices, ℓ, in the case of turbulence. Vortex lines are described as space curves $\mathbf{s}(\xi, t)$ where ξ is arclength. The equation of motion

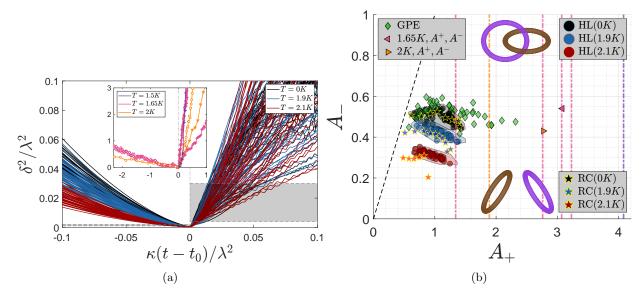(a)   (b)

FIG. 2: *(a)*: Time evolution of the (dimensionless) minimum distance squared δ^2 plotted versus (dimensionless) $\kappa(t - t_0)$ for the Hopf link reconnections at $T = 0K, 1.9K$ and $2.1K$ (black, blue and red respectively). The grey shaded areas are the regions used to estimate the prefactors $A^{\pm}$. *Inset:* Experimental superfluid helium data. *(b)*: Comparison of all prefactors: Hopf links (*HL*, circles), ring collisions (*RC*, stars with yellow outline), GPE-data from Villois *et al.* [10] (green diamonds) and experimental results from this study (triangles and vertical dot-dashed lines). The shaded areas associated with each colour represent the convex hull of errors for each temperature and the black dashed line represents the theoretical bound for A^+/A^-. Schematic rendering of initial conditions are included.

of the vortex lines is

$$\dot{\mathbf{s}}(\xi, t) = \mathbf{v}_s + \frac{\beta}{(1+\beta)} \left[\mathbf{v}_{ns} \cdot \mathbf{s}' \right] \mathbf{s}' + \beta \mathbf{s}' \times \mathbf{v}_{ns} + \beta' \mathbf{s}' \times \left[\mathbf{s}' \times \mathbf{v}_{ns} \right], \tag{2}$$

where $\dot{\mathbf{s}} = \partial \mathbf{s}/\partial t$, $\mathbf{s}' = \partial \mathbf{s}/\partial \xi$ is the unit tangent vector, $\mathbf{v}_n$ and $\mathbf{v}_s$ are the normal fluid and superfluid velocities at $\mathbf{s}$, $\mathbf{v}_{ns} = \mathbf{v}_n - \mathbf{v}_s$, and β, β' are temperature and Reynolds number dependent mutual friction coefficients [22]. The normal fluid velocity $\mathbf{v}_n$ is described as a classical fluid obeying the incompressible ($\nabla \cdot \mathbf{v}_n = 0$) Navier-Stokes equations:

$$\frac{\partial \mathbf{v}_n}{\partial t} + (\mathbf{v}_n \cdot \nabla) \mathbf{v}_n = -\frac{1}{\rho} \nabla p + \nu_n \nabla^2 \mathbf{v}_n + \frac{\mathbf{F}_{ns}}{\rho_n}, \tag{3}$$

where $\mathbf{F}_{ns}$ is the mutual friction force that couples the normal fluid and the superfluid vortices, and acts as an internal injection mechanism. In Eq. (3), $\rho = \rho_n + \rho_s$, where ρ_n and ρ_s are the normal fluid and superfluid densities, p is the pressure, and ν_n is the kinematic viscosity of the normal fluid. Equations (2) and (3) are solved in dimensionless form by rescaling them by the characteristic time τ and length λ. The algorithm for vortex reconnections is standard [23]. We consider two distinct initial vortex configurations at three temperatures $T = 0$ K, 1.9 K and 2.1 K corresponding to the superfluid fractions $\rho_s/\rho = 100\%$, 58% and 26%. To compare with experiments, the unit of length is set to $\lambda = 1.59 \times 10^{-4}$ m, and the time units to $\tau = 0.183$ s at $T = 0$ K and 1.9 K, and $\tau = 0.242$ s at $T = 2.1$ K, see also the SM for details. All configurations lead to a vortex reconnection. The first configuration consists of two vortex rings of (dimensionless) radius $R \approx 1$ in a tent-like shape which collide obliquely making an initial angle α with the vertical direction, as shown in Fig. 1, and, schematically, in Fig. 2b. By changing the parameter α, we create a sample of 12 realizations at each temperature (again, see the SM for details). The second configuration is the Hopf link, shown schematically in Fig. 2b. It consists of two perpendicular linked rings of radius $R \approx 1$ with an offset in the xy-plane. By changing the offset, we create a sample of 49 reconnections at each temperature, as described in the SM. In all cases, normal fluid structures generated by moving superfluid vortex rings [24], are initially prepared to eliminate any potential transients.

Scaling law. — In the experiment, two reconnections were observed where both A^+ and A^- could be identified and calculated, at $T = 1.65K$ and $T = 2K$, plotted as orange triangles in Fig. 2b. We also analysed six additional experimental observations of the *post-reconnection* dynamics only (vertical dot-dashed lines). All were consistent with the $\delta^{1/2}$ scaling with A^+ in the range 1.2-4.2, plotted as vertical lines in Fig. 2b Their corresponding minimal
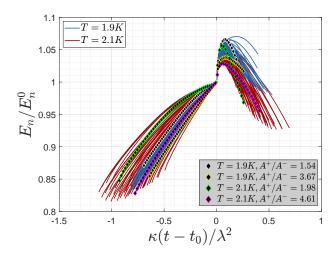
FIG. 3: Normal fluid kinetic energy E_n scaled by E_n^0 (the kinetic energy at $t = t_0$), plotted versus (dimensionless) $\kappa(t - t_0)$ for the Hopf link reconnections. Black diamonds represent the simulations with minimum and maximum prefactor ratios A^+/A^- at $T = 1.9$ K and $T = 2.1$ K respectively.

distances are displayed in the inset of Fig 2a. The pre-reconnection factor A^- lies within the 0.4-0.6 range, consistent with the results of the numerics, and a clear temperature effect between a superfluid component majority and normal fluid component majority. In the case of the Hopf link we have performed 147 simulations (49 across 3 temperatures) as shown in Fig. 2a and verified Eq. (1) for the minimum distance $\delta^\pm$. The prefactors $A^\pm$ have been computed in the shaded region of the figure. In the pre-reconnection regime ($t < t_0$) we observe a clear segregation of the values of A^- due to temperature: the minimum distance grows more rapidly with time if the temperature is lowered. In stark contrast, there is almost no memory of the temperature in the post-reconnection regime ($t > t_0$).

At $T = 0$ K, our calculations for superfluid helium (black symbols in Fig. 2b) are in good agreement with previous results obtained with the GPE [10] (green diamonds), showing irreversible dynamics. In addition, the computed values of $A^- \approx 0.4$-0.6 at $T = 0$ K are consistent with analytical calculations [25, 26]. At non-zero temperatures, our results confirm the irreversibility of vortex reconnections observed at $T = 0$ as A^+ is always larger than A^-. Importantly, this asymmetry is recovered in all our simulations, regardless of their initial condition. The same asymmetry between A^+ and A^- at non-zero temperatures has been observed for reconnections in finite-temperature Bose-Einstein condensatates [27], although in this work the system is not homogeneous (the condensate is confined by a harmonic trap) and the thermal component is a ballistc gas, not a viscous fluid. Note that the vortex reconnections in classical viscous fluids reported in [9] also display a clear 1/2 power-law scaling for the minimum distance with $A^- \approx 0.3$-0.4, which again shows good agreement with our results. The scaling law (Eq. 1) and the range of values of A^- hence appear to have a universal character in vortex reconnections, independently of the nature of the fluid, classical or quantum.

Energy injection. — The normal fluid impacts the dynamics of reconnecting superfluid vortices via the temperature dependent mutual friction coefficients. Conversely, the motion of superfluid vortices involved in the reconnection process influence, significantly, the dynamics of the normal fluid. Figure 3 indeed shows that the normal fluid energy, E_n, suddenly increases at the reconnection time by an amount ($\approx 5\%$) which is smaller but comparable to the continuous energy increase as vortex lines approach each other. Indeed the curvature $\zeta = |\mathbf{s}''|$ of the vortex line spikes at $t = t_0$ when the reconnection cusp is created, and, in the first approximation [28], the magnitude of the energy injected in the normal fluid per unit time I is proportional to the strength of the mutual friction force $\mathbf{F}_{ns}$ which scales as $|\mathbf{F}_{ns}(\mathbf{s})| \propto |\dot{\mathbf{s}} - \mathbf{v}_n| \propto |\dot{\mathbf{s}}| \propto \zeta$. This sudden transfer of energy [29] from the superfluid vortex configuration to the normal fluid is the origin of the small scale normal fluid enstrophy structures which are visible in Fig. 1.

The total energy injected into the normal fluid by the reconnection, ΔE_n, which hereafter we refer to as the energy jump, is defined as

$$\Delta E_n = \max\left[E_n(t > t_0)\right] - E_n^0, \tag{4}$$

where $E_n^0 = E_n(t_0)$ is the normal fluid kinetic energy at $t = t_0$. Normalized energy jumps are plotted in Fig. 4 as a function of the ratio A^+/A^-. Here, we observe that the larger A^+/A^- is, the smaller the normal fluid excitation is.

The emission of the sound pulse at the vortex reconnection [12] which is typical of the GPE model is absent in our incompressible hydrodynamic approach. To model this effect, the change of vortex length, ΔL, created by the vortex reconnection algorithm is always negative by construction [23], because, in the local induction approximation
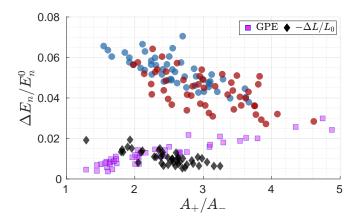
FIG. 4: Normalized energy jumps $\Delta E_n/E_n^0$ for Hopf link reconnections.The solid black diamonds are the normalized change in line length $\Delta L/L_0$ in the $T = 0$ K case. Blue and red circle correspond to $T = 1.9K$ and $T = 2.1K$,respectively. The purple squares are from GPE simulations of Villois et al. [10].

to the Biot-Savart law, the superfluid incompressible kinetic energy, E_s, is proportional to the vortex length, L. Such procedure ensures that at $T = 0$ K when a reconnection occurs $\Delta E_s \propto \Delta L < 0$. Consequentially, in the absence of any dissipative normal fluid, the superfluid energy E_s that would be transferred to the sound pulse, normalized with its value E_s^0 at reconnection, is $-\Delta L/L_0$., If these normalized energy jumps (black diamonds in Fig. 4) are compared to the results obtained with the compressible GPE [10] (purple squares) we find a good agreement, confirming that the model we employ, is suitable for the investigation of the feature of single reconnection events.

Implications for turbulence. — Our numerical results have implications for our understanding of quantum turbulence [30]. A fully developed turbulent tangle of vortices is characterized by its vortex line density $\mathcal{L}$ (vortex length per unit volume); the frequency of vortex reconnections per unit volume is $f = (\kappa/6\pi)\mathcal{L}^{5/2}\ln(\mathcal{L}^{-1/2}/a_0)$ [31]. From Fig. 3 we estimate the normal fluid reconnection relaxation time τ_n as the time after reconnection at which the normal fluid energy E_n/E_0 has decayed to the pre-reconnection level: in our dimensionless units, $\kappa\tau_n \approx 0.25$. Using this timescale, we estimate that the average vortex line density that is required to sustain the normal fluid in a perturbed state via frequent vortex reconnections is approximately $\mathcal{L} \approx 10^7$ to $10^8 \mathrm{m}^{-2}$. Experiments in ^{4}He [32–36] and in ^{3}He [37] can achieve vortex line densities much larger than this.

Conclusions. — We have conducted an experiment using passive particle tracers and a suite of numerical simulations of vortex reconnections over a wide range of temperatures using a model of ^{4}He which accounts for the coupled dynamics of superfluid and normal fluid components. We have verified the scaling law of the minimum vortex distance $\delta^{\pm} = A^{\pm}(\kappa|t - t_0|)^{1/2}$ and found that the approach prefactor A^- has a clear temperature dependence independent of the geometry in both experiments and numerics, in contrast to the separation prefactor A^+. The prefactors are in good agreement with GPE simulations [10, 27] and classical fluid reconnections [9] revealing that vortex reconnections display a universal behaviour, linked to irreversible vortex energy dissipation, regardless of the nature of the fluid (classical or quantum) and of temperature, *i.e.* regardless of the small scale energy transfer mechanism. It is worth noting that the behaviour, as a function of A^+/A^-, of the energy injected in the normal fluid (at $T > 0$) and of the energy transferred to sound (at $T = 0$) [10, 12] is dissimilar: the former decreases as A^+/A^- increases, the latter the opposite. This likely arises from the distinct physics governing the loss of superfluid incompressible kinetic energy: mutual friction at $T > 0$, quantum pressure at $T = 0$. We have also found that a reconnection event suddenly injects an amount of energy into the normal fluid which is comparable to the energy transferred by friction during the vortex approach. Applying these results to turbulence, we have compared the decay time of the normal fluid structures created by a reconnection to the frequency of reconnections in a vortex tangle, and argued that, if the vortex line density is large enough, these punctuated energy injections should sustain the normal fluid in a perturbed state, which may lead to a new type of turbulence.

program" on complex systems.

---

[1] J. Yao and F. Hussain, Vortex reconnection and turbulence cascade, Ann. Rev. Fluid Mech. **54**, 317 (2022).

[2] I. T. Chapman, R. Scannell, W. A. Cooper, J. P. Graves, R. J. Hastie, G. Naylor, and A. Zocco, Magnetic reconnection triggering magnetohydrodynamic instabilities during a sawtooth crash in a tokamak plasma, Phys. Rev. Lett. **105**, 255002 (2010).

[3] S. Nazarenko and R. West, Analytical solution for nonlinear Schrödinger vortex reconnection, J. Low Temp. Phys. **132**, 1 (2003).

[4] G. P. Bewley, M. S. Paoletti, K. R. Sreenivasan, and D. P. Lathrop, Characterization of reconnecting vortices in superfluid helium, Proc. Nat. Acad. Sci. USA **105**, 13707 (2008).

[5] M. S. Paoletti, M. E. Fisher, and D. P. Lathrop, Reconnection dynamics for quantized vortices, Physica D **239**, 1367 (2010).

[6] S. Zuccher, M. Caliari, A. W. Baggaley, and C. F. Barenghi, Quantum vortex reconnections, Phys. Fluids **24**, 125108 (2012).

[7] A. Villois, D. Proment, and G. Krstulovic, Universal and nonuniversal aspects of vortex reconnections in superfluids, Phys. Rev. Fluids **2**, 044701 (2017).

[8] L. Galantucci, A. W. Baggaley, N. G. Parker, and C. F. Barenghi, Crossover from interaction to driven regimes in quantum vortex reconnections, Proc. Nat. Acad. Sci. USA **116**, 12204 (2019).

[9] J. Yao and F. Hussain, Separation scaling for viscous vortex reconnection, J. Fluid Mech. **900**, R4 (2020).

[10] A. Villois, D. Proment, and G. Krstulovic, Irreversible dynamics of vortex reconnections in quantum fluids, Phys. Rev. Lett. **125**, 164501 (2020).

[11] D. Proment and G. Krstulovic, Matching theory to characterize sound smission during vortex reconnection in quantum fluids, Phys. Rev. Fluids **5**, 104701 (2020).

[12] M. Leadbeater, T. Winiecki, D. C. Samuels, C. F. Barenghi, and C. S. Adams, Sound emission due to superfluid vortex reconnections, Phys. Rev. Lett. **86**, 1410 (2001).

[13] M. S. Paoletti, M. E. Fisher, K. R. Sreenivasan, and D. P. Lathrop, Velocity statistics distinguish quantum turbulence from classical turbulence, Physical review letters **101**, 154501 (2008).

[14] W. Guo, M. La Mantia, D. P. Lathrop, and S. W. Van Sciver, Visualization of two-fluid flows of superfluid helium-4, Proceedings of the National Academy of Sciences **111**, 4653 (2014).

[15] C. Peretti, J. Vessaire, Émeric Durozoy, and M. Gibert, Direct visualization of the quantum vortex lattice structure, oscillations, and destabilization in rotating ¡sup¿4¡/sup¿he, Science Advances **9**, eadh2899 (2023), https://www.science.org/doi/pdf/10.1126/sciadv.adh2899.

[16] T. Xu and S. W. Van Sciver, Density effect of solidified hydrogen isotope particles on particle image velocimetry measurements of He II flow, AIP Conf. Proc. **985**, 191 (2008).

[17] Y. Tang, W. Guo, H. Kobayashi, S. Yui, M. Tsubota, and T. Kanai, Imaging quantized vortex rings in superfluid helium to evaluate quantum dissipation, Nat. Commun. **14**, 2941 (2023).

[18] Y. Tang, S. Bao, and W. Guo, Superdiffusion of quantized vortices uncovering scaling laws in quantum turbulence, Proc. Natl. Acad. Sci. U.S.A. **118**, e2021957118 (2021).

[19] E. Fonda, K. R. Sreenivasan, and D. P. Lathrop, Sub-micron solid air tracers for quantum vortices and liquid helium flows, Rev. Sci. Instrum. **87**, 025106 (2016).

[20] U. Giuriato and G. Krstulovic, Quantum vortex reconnections mediated by trapped particles, Phys. Rev. B **102**, 094508 (2020).

[21] KW. Schwarz, Three-dimensional vortex dynamics in superfluid ^{4}He, Phys. Rev. B **38**, 2398 (1988).

[22] L. Galantucci, A. W. Baggaley, C. F. Barenghi, and G. Krstulovic, A new self-consistent approach of quantum turbulence in superfluid helium, Eur. Phys. J. Plus **135**, 547 (2020).

[23] A. W. Baggaley, The sensitivity of the vortex filament method to different reconnection models, J. Low Temp. Phys. **168**, 18 (2012).

[24] D. Kivotides, C. F. Barenghi, and D. C. Samuels, Triple vortex ring structure in superfluid helium ii, Science **290**, 777 (2000).

[25] L. Boué, D. Khomenko, V. L'vov, and I. Procaccia, Analytic solution of the approach of quantum vortices towards reconnection, Phys. Rev. Lett. **111**, 145302 (2013).

[26] R. S, Self-similar vortex reconnection, C. R. Méc **347**, 365 (2019).

[27] A. J. Allen, S. Zuccher, M. Caliari, N. P. Proukakis, N. G. Parker, and C. F. Barenghi, Vortex reconnections in atomic condensates at finite temperature, Phys. Rev. A **90**, 013601 (2014).

[28] L. Galantucci, G. Krstulovic, and C. Barenghi, Friction-enhanced lifetime of bundled quantum vortices, Phys. Rev. Fluids **8**, 014702 (2023).

[29] P. Z. Stasiak, A. W. Baggaley, G. Krstulovic, C. F. Barenghi, and L. Galantucci, Cross-component energy transfer in superfluid helium-4, J. Low Temp. Phys. (2024).

[30] C. F. Barenghi, L. Skrbek, and K. R. Sreenivasan, *Quantum Turbulence* (Cambridge University Press, 2023).

[31] C. F. Barenghi and D. C. Samuels, Scaling laws of vortex reconnections, J. Low Temp. Phys. **136**, 281 (2004).

[32] K. W. Schwarz and C. W. Smith, Pulsed-ion study of ultrasonically generated turbulence in superfluid 4He, Physics Letters A **82**, 251 (1981).

[33] F. P. Milliken, K. W. Schwarz, and C. W. Smith, Free Decay of Superfluid Turbulence, Phys. Rev. Lett. **48**, 1204 (1982).

[34] P.-E. Roche and C. F. Barenghi, Vortex spectrum in superfluid turbulence: Interpretation of a recent experiment, EPL **81**, 36002 (2008).

[35] P.-E. Roche, P. Diribarne, T. Didelot, O. Français, L. Rousseau, and H. Willaime, Vortex density spectrum of quantum turbulence, EPL **77**, 66002 (2007).

[36] S. Babuin, E. Varga, L. Skrbek, E. Lévêque, and P.-E. Roche, Effective viscosity in quantum turbulence: a steady state approach, Europhys. Lett. **106**, 24006 (2014).

[37] D. I. Bradley, D. O. Clubb, S. N. Fisher, A. M. Guénault, R. P. Haley, C. J. Matthews, G. R. Pickett, V. Tsepelin, and K. Zaki, Decay of pure quantum turbulence in superfluid ^{3}He-B, Phys. Rev. Lett. **96**, 035301 (2006).

[38] L. Galantucci, M. Sciacca, and CF. Barenghi, Coupled normal fluid and superfluid profiles of turbulent helium II in channels, Phys Rev B **92**, 174530 (2015).

SUPPLEMENTARY MATERIALS

Appendix A: Experimental Method

To produce solidified deuterium (D_2) tracer particles, we slowly inject a gas mixture of 5% D_2 and 95% ^{4}He into a superfluid helium bath. Our gas injection system is similar to that described by Fonda et al. [19]. A solenoid valve is installed to control the duration of the gas injection, and a needle valve is used to regulate the gas flow rate. The injected D_2 gas solidifies into small ice particles with a mean radius of 1.1 μm, derived from the particle settling velocities in quiescent superfluid helium [17]. A 473 nm continuous-wave laser sheet (thickness: 0.8 mm) illuminates the particles, and their motion in the laser sheet plane is recorded by a camera at 200 frames per second with a maximum resolution of 2560×1440 pixels. We then identify vortex reconnection events from the recorded videos, and manually track the coordinates of the trapped particles for the pre- (if captured) and post-reconnection. Knowing the particle coordinates, the minimum distance between the reconnecting vortices $\delta^{\pm}(t)$ can be measured. We calculate the prefactors $A^{\pm}$ using the slopes of linear fits to the $\delta^2(t)$ data.

Appendix B: Numerical Method

Using Schwarz mesoscopic model [21], vortex lines can be described as space curves $\mathbf{s}(\xi, t)$ of infinitesimal thickness, with a single quantum of circulation $\kappa = h/m_4 = 9.97 \times 10^{-8} \mathrm{m}^2/\mathrm{s}$, where h is Planck's constant, $m_4 = 6.65 \times 10^{-27}\mathrm{kg}$ is the mass of one helium atom, ξ is the natural parameterisation, arclength, and t is time. These conditions are a good approximation, since the vortex core radius of superfluid ^{4}He($a_0 = 10^{-10}$m) is much smaller than any of the length scale of interest in turbulent flows. The equation of motion is

$$\dot{\mathbf{s}}(\xi, t) = \mathbf{v}_s + \frac{\beta}{1+\beta}\left[\mathbf{v}_{ns} \cdot \mathbf{s}'\right]\mathbf{s}' + \beta\mathbf{s}' \times \mathbf{v}_{ns} + \beta'\mathbf{s}' \times \left[\mathbf{s}' \times \mathbf{v}_{ns}\right], \tag{B1}$$

where $\dot{\mathbf{s}} = \partial\mathbf{s}/\partial t$, $\mathbf{s}' = \partial\mathbf{s}/\partial\xi$ is the unit tangent vector, $\mathbf{v}_{ns} = \mathbf{v}_n - \mathbf{v}_s$, $\mathbf{v}_n$ and $\mathbf{v}_s$ are the normal fluid and superfluid velocities at $\mathbf{s}$ and β, β' are temperature and Reynolds number dependent mutual friction coefficients [22]. The superfluid velocity $\mathbf{v}_s$ at a point $\mathbf{x}$ is determined by the Biot-Savart law

$$\mathbf{v}_s(\mathbf{x}, t) = \frac{\kappa}{4\pi}\oint_{\mathcal{T}}\frac{\mathbf{s}'(\xi, t) \times [\mathbf{x} - \mathbf{s}(\xi, t)]}{|\mathbf{x} - \mathbf{s}(\xi, t)|}d\xi, \tag{B2}$$

where $\mathcal{T}$ represents the entire vortex configuration. There is currently a lack of a well-defined theory of vortex reconnections in superfluid helium, like for the Gross-Pitaevskii equation [7, 10, 11]. An *ad hoc* vortex reconnection algorithm is employed to resolve the collisions of vortex lines [23].
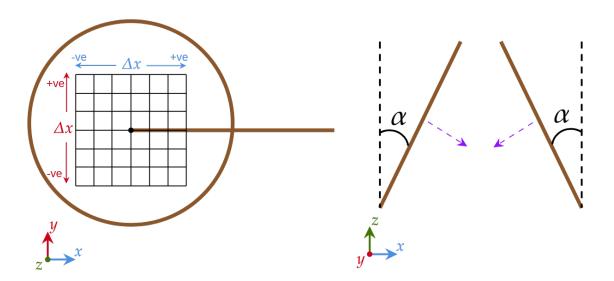

FIG. 5: Schematic diagram for numeric initial condition. *Left:* Hopf-link. *Right:* Oblique collision.

A *two-way model* is crucial to understand the accurately interept the back-reaction effect of the normal fluid on the vortex line and vice-versa [29]. We self-consistently evolve the normal fluid $\mathbf{v}_n$ with a modified Navier-Stokes equation

$$\frac{\partial \mathbf{v}_n}{\partial t} + (\mathbf{v}_n \cdot \nabla)\mathbf{v}_n = -\nabla \frac{p}{\rho} + \nu_n \nabla^2 \mathbf{v}_n + \frac{\mathbf{F}_{ns}}{\rho_n}, \tag{B3}$$

$$\mathbf{F}_{ns} = \oint_{\mathcal{T}} \mathbf{f}_{ns}\delta(\mathbf{x} - \mathbf{x})d\xi, \quad \nabla \cdot \mathbf{v}_n = 0, \tag{B4}$$

where $\rho = \rho_n + \rho_s$ is the total density, ρ_n and ρ_s are the normal fluid and superfluid densities, p is the pressure, ν_n is the kinematic viscosity of the normal fluid and $\mathbf{f}_{ns}$ is the local friction per unit length [38]

$$\mathbf{f}_{ns} = -D\mathbf{s}' \times [\mathbf{s}' \times (\dot{\mathbf{s}} - \mathbf{v}_n)] - \rho_n \kappa \mathbf{s}' \times (\mathbf{v}_n - \dot{\mathbf{s}}), \tag{B5}$$

where D is a coefficient dependent on the vortex Reynolds number and intrinsic properties of the normal fluid.

The results in this Letter are reported in dimensionless units, where the characteristic length scale is $\tilde{\lambda} = D/D_0$, where $D^3 = (1 \times 10^{-3}\text{m})^3$ is the dimensional cube size, $D_0^3 = (2\pi)^3$ is the non-dimensional cubic computational domain. The time scale is given by $\tilde{\tau} = \tilde{\lambda}^2 \nu_n^0/\nu_n$, where the non-dimensional viscosity ν_n^0 resolves the small scales of the normal fluid. In these simulations, these quantities are $\tilde{\lambda} = 1.59 \times 10^{-4}\text{cm}$, $\nu_n^0 = 0.16$ and $\tilde{\tau} = 0.183\text{s}$ at $T = 0K$ and at $T = 1.9K$ and $\tilde{\tau} = 0.242\text{s}$ at $T = 2.1K$. We consider two distinct initial vortex geometries at $T = 0K, 1.9K$ and $2.1K$. The first is a Hopf link, two linked rings of radius $R \approx 1$ with an offset in the xy-plane defined by parameters Δl_x and Δl_y. The offsets are chosen so that $(\Delta l_x, \Delta l_y) \in \{(0.125i, 0.125j)|i, j = -3, \cdots, 3\}$, a total of 49 reconnections for each temperature. The second geometry is a collision of vortex rings of radius $R \approx 1$ in a tent-like configuration (see Fig. 5), making an angle α with the vertical. We take 12 realisations of α, such that $\alpha \in \{i\pi/13|i = 1, \cdots, 12\}$.

In both cases, normal fluid rings are initially superimposed to match the vortex lines, eliminating the transient phase of generating normal fluid structures. The Lagrangian discretisation of vortex lines is $\Delta\xi = 0.025$ (a total of 668 discretiation points) with a timestep of $\Delta t_{VF} = 1.25 \times 10^{-5}$. A total of $N = 256^3$ Eulerian mesh points were used for the normal fluid, with a timestep of $\Delta t_{NS} = 40\Delta t_{VF}$.